Piezoelectric co-axial filaments produced by co-extrusion of poly(vinylidene fluoride) and electrically conductive inner and outer layers

R. S. Martins[1]; R. Gonçalves[2]; J. G. Rocha[3]; J. M. Nóbrega[1]; H. Carvalho[4] and S. Lanceros-Mendez[2]

[1] *IPC/I3N – Institute for Polymers and Composites, University of Minho, Campus de Azurém, 4800-058 Guimarães, Portugal*

[2] *Centro/Departamento de Física, University of Minho, Campus de Gualtar, 4710-058 Braga, Portugal*

[3] *Dep. Industrial Electronics, University of Minho, 4800-058 Guimarães, Portugal*

[4] *Dep. Textile Engineering, University of Minho, Campus de Azurém, 4800-058 Guimarães, Portugal*

ABSTRACT

The development of new thermoplastic polymer-based piezoelectric sensors with filament geometry is described. These filaments are appropriate for integration into textiles and provide new possibilities in the design and development of low cost flexible sensors produced at high rates. The developed three-layered piezoelectric monofilaments have been produced by co-extrusion using poly(vinylidene fluoride) and two different polypropylene-based electrically conductive polymers. Filaments with about 800 μm diameter, producing electrical signals proportional to the mechanical deformation applied, were obtained. The signal output has been found sufficient for straightforward use with conventional piezoelectric signal conditioning systems. One of the conductive polymers tested allowed better filament geometry and process stability.

This paper describes the co-extrusion production process and the results obtained in the electromechanical tests performed.

KEYWORDS: piezoelectric sensors; extrusion; ferroelectrics; polymers; PVDF; PP; piezoelectric properties

1. INTRODUCTION

Poly(vinylidene fluoride) (PVDF) has been extensively studied due to its remarkable piezo-, pyro- and ferroelectric properties among polymers. These properties have been used for the development of sensor and actuator devices and technologies.[1-3]

The electroactive properties of PVDF depend on several factors including the degree of crystallinity, structure and orientation of the crystalline fraction of the semi-crystalline polymer, which strongly depend on the employed processing conditions.[1,3-12]

PVDF can crystallize in four different crystalline phases, identified as α, β, γ and δ. The non-polar α-phase is readily obtained by crystallization from the melt at high or moderate cooling speeds.[1,3] From the point of view of its piezoelectric activity, the most interesting phase is the β-phase, which is most commonly obtained by stretching the α-PVDF at temperatures between 80 ºC and 120 ºC with a stretch ratio (R) between 3 and 5.[1,11,12]

After processing, the material is usually further poled in order to improve its piezoelectric response, aiming for the production of better sensor and actuator devices. After this stage, the piezoelectric polymer will produce an electrical potential upon mechanical excitation and a mechanical action will be produced if the polymer is subjected to an electric field. Poling can be achieved using several alternatives, including corona poling and the Bauer method, among others.[1-3] The most simple and straightforward poling method is performed just by applying to the electroded material

an electrical field higher than its coercive field, which typically ranges from 50 to 120 MV m^{-1} for PVDF.[13] If the poling is undertaken in a temperature range between 85 ºC and 130 ºC, the piezoelectric response can be further improved.[14]

PVDF-based piezoelectric sensors and actuators are available on the market, usually in the form of films. A polymer based piezoelectric device is composed of at least one piezoelectric active layer and two electrically conductive layers used as electrodes for the connection of electronic conditioning/drive equipment.[15]

In the case of films, the typical arrangement of the layers is the parallel one (see Figure 1). In this work, piezoelectric filaments comprising three thermoplastic material layers in coaxial arrangement, as illustrated in Figure 1, have been developed. This geometry is expected to allow a new range of applications in areas such as e-textiles and structural health monitoring.

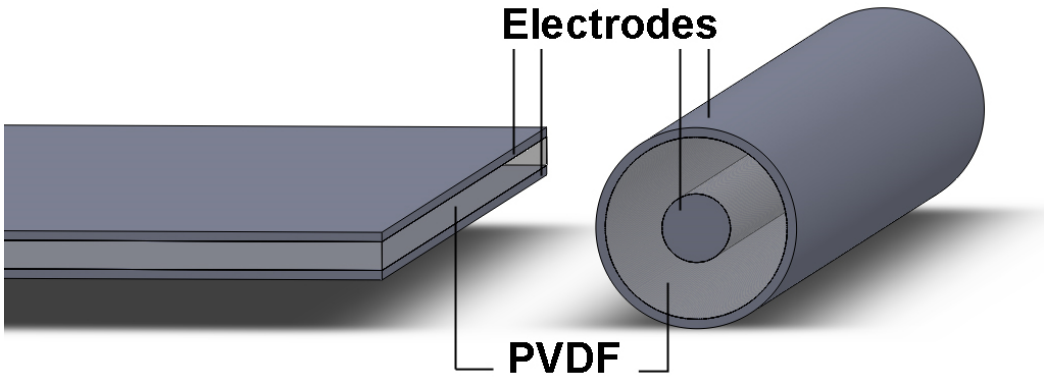

FIGURE 1 Parallel (film) and coaxial (filament) arrangement of layers

An effective way to achieve the desired geometry is to process simultaneously the conductive elements and the piezoelectric layer. One of the most interesting possibilities is the use of polymer based electrodes, in particular the ones based on polypropylene. Polypropylene has a very competitive cost, based on the cheap monomer and the efficient polymerization technology, when compared with other polymers.[16] It can be easily processed by extrusion and the addition of a small amount of conductive fillers,

allows the achievement of electrically conductive thermoplastic composites.[17] Several thermoplastic polymer based conductive grades are commercially available.

The extrusion of PVDF in the form of filament and the relationship between processing parameters and the β-phase content has been investigated in some works. Some authors have concluded that the optimized processing conditions for single PVDF monofilaments are similar to the ones established for film extrusion, i.e. stretching the α-PVDF at temperatures between 80 ºC and 120 ºC using a stretch ratio between 3 and 5.[11,12,18,19]

For the production of multilayered filaments (see Figure 1) studies have been focused on the investigation of the influence of a conductive inner core on the β-phase content of PVDF. In one study, filaments have been co-extruded with a Polyproplylene/Carbon Black conductive inner core and a PVDF outer layer, and it has been shown that the electroactive phase content is not affected by the presence of the conductive inner core, and, in fact, depends just on the stretch temperature and ratio, as previously stated for mono-material filaments.[20] Similar work has been comprehensively described.[21]

With respect to the electroactive properties of the extruded filaments , a piezoelectric cable obtained from a two layer coextruded filament, comprising an internal semiconductive electrode and a PVDF layer, coated with a thin layer of a semiconductive copper based lacquer, was tested and characterized.[22] A non-linear relationship between the electrical charge produced by the cable and the force applied was determined.

Mazurek et al. describe the production of concentric piezoelectric cables by co-extrusion.[23] The outer electrode is applied in an additional step. The cables were poled using the thermoelectret method, the breakdown method, the low-temperature plasma

method and the corona method. The low-temperature plasma method produced the best piezoelectric response.

The development of piezoelectric cables using sequential processing techniques was also described.[24] An inner conductive core is covered with PVDF, which is then electroded with a metal or a semiconducting polymer and mechanically strengthened with a polymer coating. The influence of several parameters on the β-phase content of PVDF such as processing temperature, stretch ratio and cooling temperature of the PVDF after stretching, as well as the influence of the thermal impact of the coating step used to apply the outer electrode, were studied. It was found that the β-phase content increased by from 20 to 100% when stretch ratios varied between 3 and 5. A reduction of the cooling temperature from 5 ºC to -30 ºC produced an increase to 100 % of β-phase content, from 61 and 71%, depending on the inner core material. The thermal impact of the coating procedure resulted in a significant decrease of β-phase content, from 100% to a value varying between 79% and 49 %.

Vatansever et al. reports the production of PVDF monofilaments, which are stretched and poled inline by an electric field produced between two parallel plates.[25] A functional prototype of a sensor based on the material produced was achieved by placing a number of filaments in a parallel arrangement and providing copper electrodes on the upper and lower faces of the assembly. The assembly was shown to produce an electrical signal upon mechanical shock

Walter et al. manufactured a composite product comprising PVDF filaments and epoxy resin, with the filaments laid out in a parallel arrangement. The composite was then poled with a linear electric field in a direction perpendicular to the fibres.[26] Piezoelectric activity was shown both for longitudinal and bending deformations.

Piezoelectric multilayer fibres have also been produced by Egusa et al., who presented a production process involving the creation of a macroscopic pre-form of the fibre.[27,28] This pre-form is achieved by assembling the layers composing the fibre in a flat arrangement and rolling them together to produce the pre-form. The pre-form is then drawn, reaching its final dimensional (and in the case of piezoelectric fibres, also functional) state after the drawing process. This process allows the production of tens of metres of fibre in each cycle, but it does not allow a continuous production of the filament. Fibres of different, very complex structures and cross-sections have been employed, showing a piezoelectric response and acoustic transduction from kilohertz to megahertz frequencies.

Unlike to all the works previously presented, in which the filaments are obtained in discrete production steps, in this work the conductive and piezoelectric layers (Figure 1) are produced by co-extrusion, in a single operation. This strategy represents a significant reduction of the processes involved in the manufacturing process.

The remainder of this paper is organized as follows: Section 2 describes the materials employed and the production and characterization methods, while in Section 3 the main results are presented and discussed. The paper ends with the main conclusion of the work.

2. EXPERIMENTAL

2.1. Filament production

The piezoelectric filament is composed by a PVDF layer surrounded by two conductive layers in a coaxial arrangement (Figure 1).

Two different co-extruded filaments were produced using Solvay Solef Ta-1010 PVDF for the piezoelectric layer. For the electrode layers, two different compounds were used: Pre-Elec 1396 conductive PP, from Premix, and PlastiCyl PP2001, from Nanocyl. The

latter, a carbon nanotube-based compound is supplied in a 20 %wt master batch and was mixed on a Leistritz twin-screw extrusion line, employing PP Moplen HP540J from LyondellBasell, to achieve a 7 %wt concentration for the filler, and granulated using a conventional granulator (C F SCHEER & CIE, Model D-7000). The two filaments will hereinafter be designated as type 1 (extruded using the Premix compound) and type 2 (extruded using the Nanocyl compound).

The three-layer filaments were then produced in a prototype monofilament co-extrusion line schematically illustrated in Figure 2.

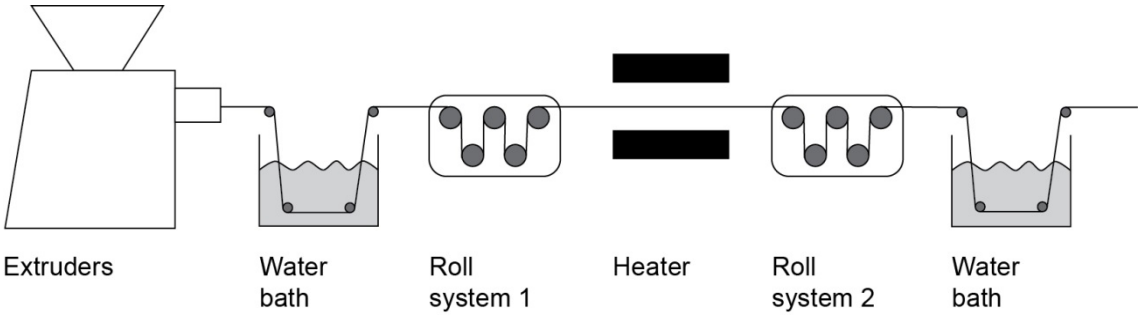

FIGURE 2 Monofilament prototype co-extrusion line used for the production of the filaments.

In this line, two extruders were employed, since two different materials are required to produce the desired filaments. In the system, the materials are pumped at a pre-defined rate by the extruders, employing the processing conditions shown in Table 1, through a co-extrusion die, illustrated in Figure 3, which shapes the multilayer coextruded filaments.

TABLE 1 Processing conditions employed on the production of the filaments

Conditions	Filament type 1	Filament type 2
Extrusion temperature (at die) PVDF	235 ºC	235 ºC
Extrusion temperature (at die) Conductive PP	255 ºC	255 ºC
Extruder screw speed PVDF	5 rpm	5 rpm
Extruder screw speed Conductive PP	10 rpm	10 rpm

Stretch ratio	4	5
Roll system 1 speed	7.5 m min^{-1}	7.5 m min^{-1}
Roll system 2 speed	30 m min^{-1}	37.5 m min^{-1}
Water bath temperature	20 ºC	20 ºC
Heater temperature	210 ºC	210 ºC

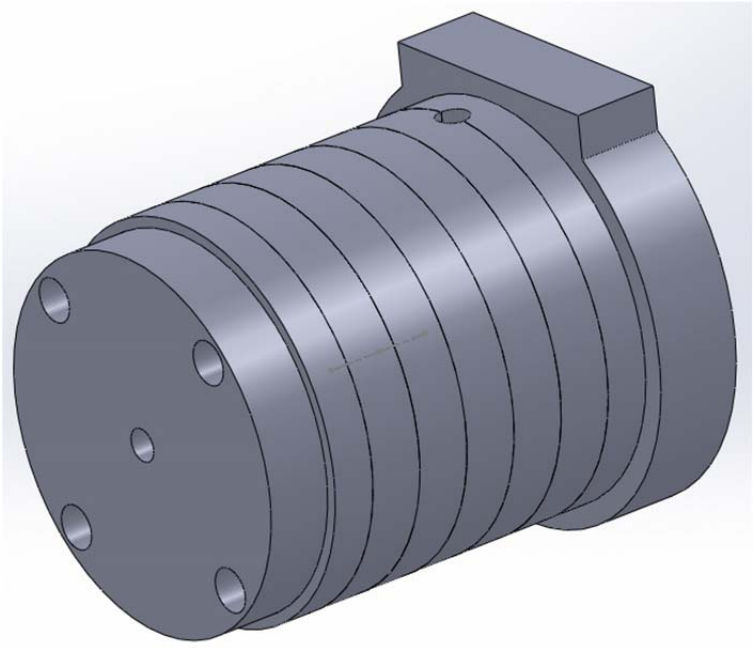

(a)

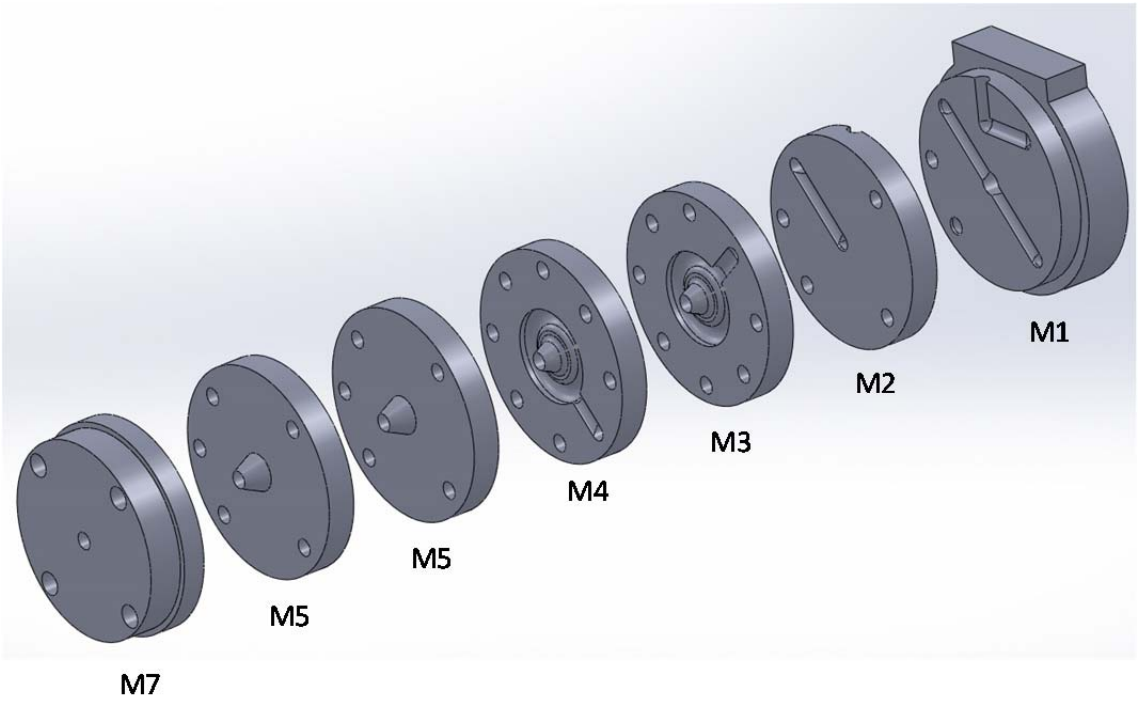

(b)

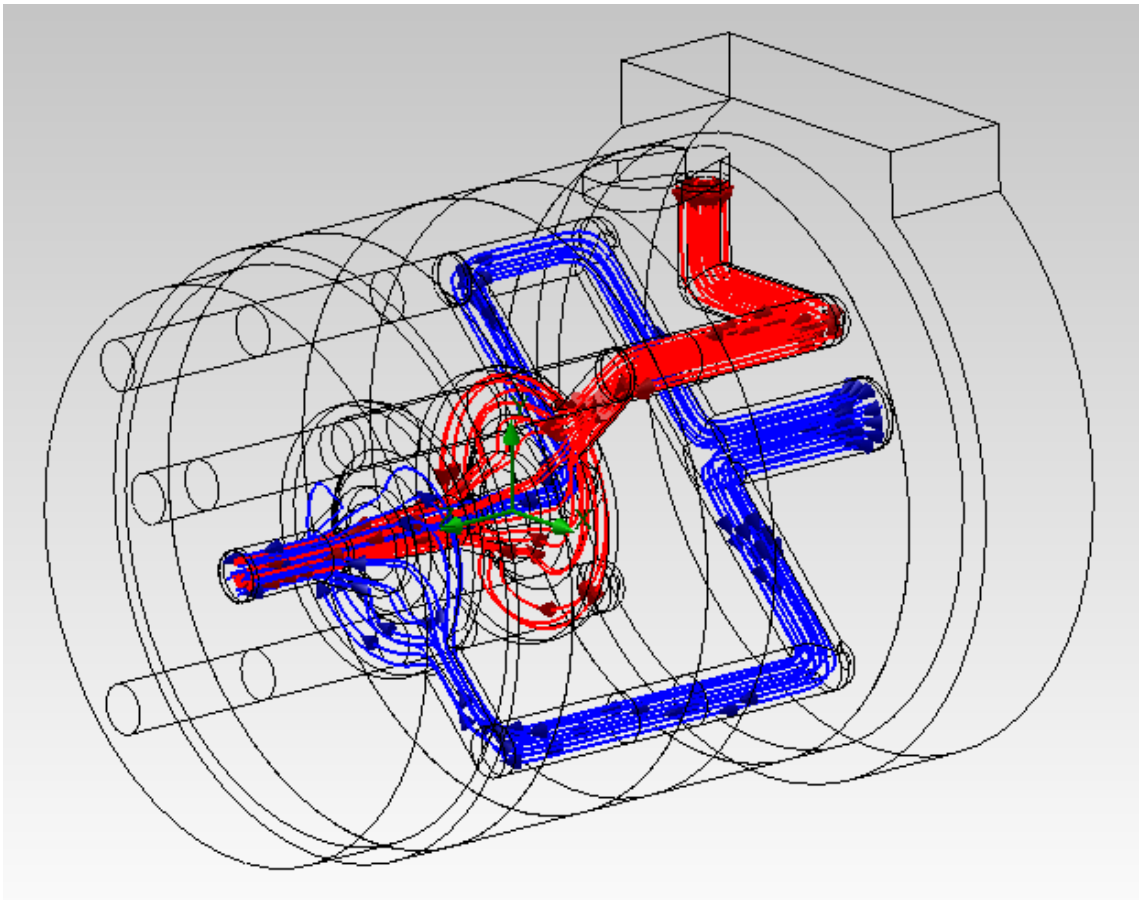

(c)

FIGURE 3 Schematic representation of the co-extrusion functional parts: (a) exploded view, (b) assembled view and (c) coextruded materials streamlines (in blue the inner and outer layers and in red the middle layer).

The modular approach of the die design allows the co-extrusion of filaments comprising up to 4 layers. The seven modules, shown in Figure 3(a), can be replaced and their positions can be switched or rotated, to produce the desired type of filament, with a specified arrangement for the layers.

The electrically conductive material (blue streamline shown in Figure 3(c)) enters the die flow channel pumped from the axially aligned extruder. This material is then divided in two independent streamlines, in order to form the two conductive layers of the filament (the inner and outer layers). The piezoelectric material (red streamline shown in Figure 3(c)) is pumped from a perpendicularly aligned extruder. The three

independent flows are then conducted to the periphery of the die, and start flowing through channels aligned in the axial direction. At the desired location, all the flow fronts are sequentially conducted to the main channel, to form the filament with the desired layer arrangement.

The depressions existing in the modules that conduct the material to form an additional layer (M3 and M5), were created to assure an even distribution of the flow along the perimeter of the layer. The modules' arrangement presented in Figure 3 allows the production of the 3 layer filament.

The die also features screws for layer thickness adjustments. These are screwed in Module M7, and can be used to adjust the flow rate independently for each streamline, by restricting the flow channel of the material that will form the respective layer.

After leaving the co-extrusion die the filament is cooled in a water bath to room temperature. Subsequently the material is drawn in a heater at a defined temperature, being the stretch ratio (*R)* determined by the relation between the linear velocities v_1 and v_2, the velocity set for roll systems 1 and 2, respectively:

$$R = \frac{v_2}{v_1} \quad (1)$$

The cooling/heating steps are required to assure a more accurate control of the drawing temperature.

An extensive experimental trial allowed establishing the optimal processing conditions for the filaments, regarding process stability and final quality of the filament. The objective was to achieve the highest drawing ratio possible at the ideal drawing temperature interval. Table 1 summarizes all the relevant processing conditions employed.

The drawing temperatures used are higher than the effective suggested temperatures found in the literature (80 to 120 ºC) but it has only been possible to draw these three-

layered filaments during production using relatively high temperatures for the Heater (Figure 3).[1-11] Using the equipment available, the process became unstable when lower temperatures were employed, with frequent filament breakage and defects. However, it should be noted that unlike in a static drawing process, in the present case the drawing is obtained in-line, thus in dynamic conditions. The filament travels through the heater at a relatively high speed, and consequently has a residence time in the heater lower than two seconds. Considering the low thermal diffusivity typical for the polymeric materials, it is obvious that the PVDF layer does not reach the temperature imposed at the heater. To assess the actual content of electroactive phase of the PVDF layer, the β-phase content was determined, as described in the next section.

2.2. Determination of β-phase content of the samples

β-phase of PVDF on the extruded filaments was characterized by Fourier transformed infrared spectroscopy (FTIR) using a Jasco FT-IR 4100 in attenuated total reflectance mode (ATR) over a range of 4000–600 cm^{-1} and sixty four scans for each sample were accumulated. For each type of filaments 5 samples were analyzed. For this characterization, 30 mm long co-extruded samples were used, from which the outer layer was removed to expose the PVDF layer, which was placed directly in the ATR device.

To quantify the amount of β-phase, infrared absorption bands at 763 and 840 cm^{-1}, specific of the α- and β-phases, were used.[29] A procedure was employed, in which the β-phase content is calculated by

$$F(\beta) = \frac{X_\beta}{X_\alpha + X_\beta} = \frac{A_\beta}{(K_\beta/K_\alpha)A_\alpha + A_\beta} = \frac{A_\beta}{1.26A_\alpha + A_\beta} \quad (2)$$

where A_α and A_β are the absorbances at 763 and 840 cm^{-1}, corresponding to the α-and β-phase material; K_α and K_β are the absorption coefficients at the respective wave numbers and X_α and X_β are the crystalline fraction of each phase. The value of K is 7.7×10^4 and 6.1×10^4 cm^2 mol^{-1} for the α- and β-phase, respectively.[1]

2.3 Filament Poling

Poling was achieved by the application of a high voltage directly to the filament. For this purpose, filaments were cut into 10 cm long segments and a high voltage source was connected between the outer and the inner conductive layer, according to the schema presented in Figure 4.

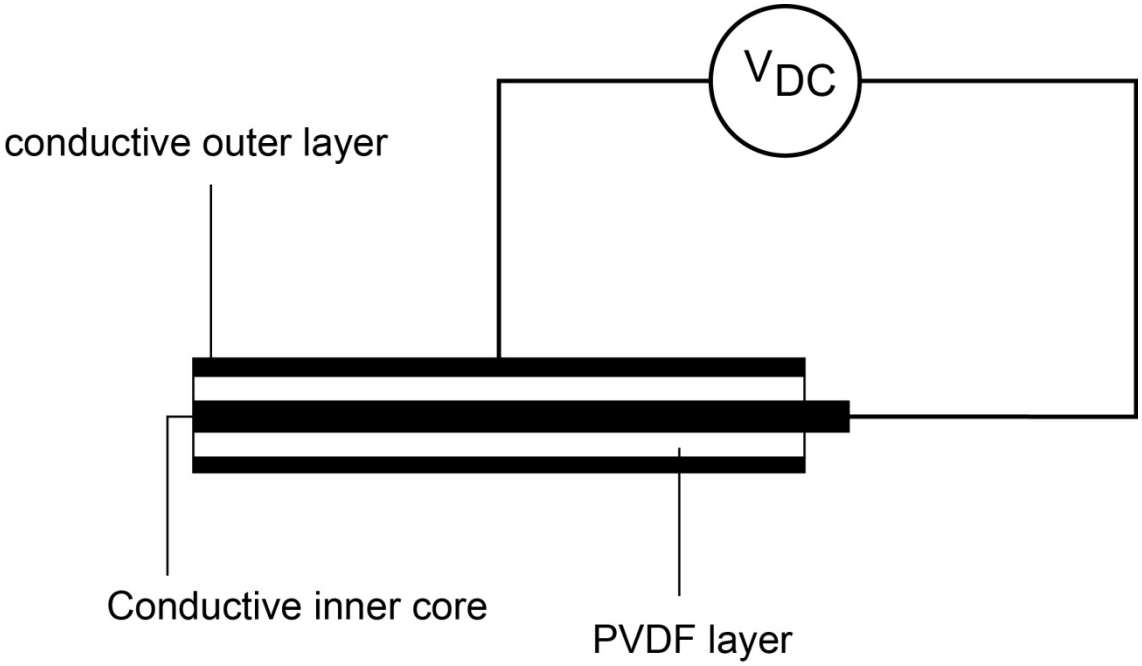

FIGURE 4 Poling scheme for the coextruded filament

The maximum voltage that could be applied on the filament poling experiments was about 9 kV. Above this value, short-circuit of the filament due to localized breakdown of the PVDF layer occurred. To increase the effectiveness of the poling, while subjected to the electrical field, the filaments were kept for 20 min at 80 ºC and then cooled to room temperature.

2.4 Mechanical characterization

Three filament samples of each of the two filament types were stretched until rupture in a universal testing machine (Shimadzu AG-IS 500 N) at a speed of 10 mm min^{-1}. The initial distance between grips was 30 mm.

2.5. Electrical evaluation

2.5.1 Signal conditioning and acquisition

For the evaluation of the potential of the extruded material for sensor applications, the filaments were connected to a custom-built charge amplifier (Figure 5).

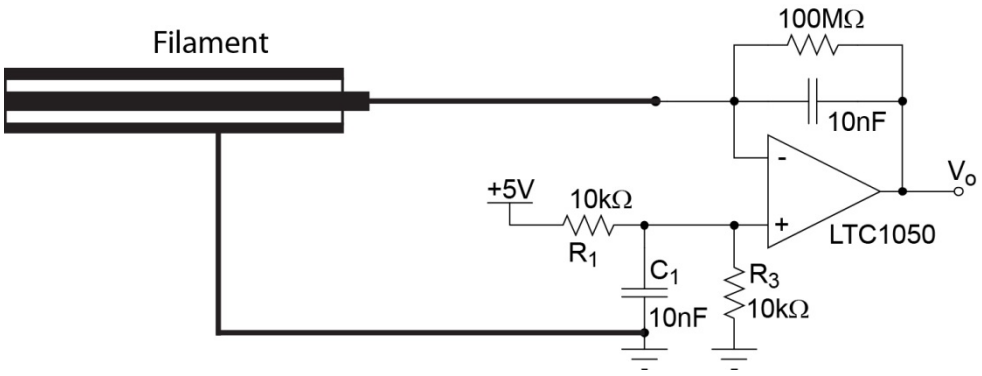

FIGURE 5 Connection and signal conditioning for the coextruded filament

In piezoelectric sensors, an electrical potential is generated upon application of mechanical action. However, the charge unbalance involved in this process is very small and is quickly dissipated in a conventional amplifier. Thus, any mechanical action produces a signal peak when the action occurs, but upon achieving a static condition no additional electrical signal is produced.

To provide a piezoelectric measurement system with the ability to measure quasi-static phenomena, or to allow it to measure slow varying stimuli, a charge-to-voltage converter, commonly known as charge amplifier, is used. In this amplifier, the charge pumped into the amplifier by the piezoelectric sensor is picked up and held in the capacitor present in the amplifier's feedback loop.

Due to the presence of bias currents, a charge amplifier with only a capacitor in its feedback loop has the tendency to saturate. To avoid this, a feedback resistor is used, which on the other hand causes the capacitor to discharge through the feedback resistor. The discharge time to 36.8 % of charge, known as the *time constant*, can be varied by adjusting the value of the component and is given by:

$$T = R_f C_f \tag{3}$$

where

T : Capacitor discharge time constant [s]
R_f : Feedback resistor value [Ω]
C_f : Feedback capacitor value [F]

A piezoelectric sensor coupled to a charge amplifier can thus be dimensioned to perform measurements of very low-frequency (or quasi-static) signals, although it is not able to measure purely static signals.[30]

The capacitor value also determines the amplifier gain, which is inversely proportional to its value:

$$G = \frac{1}{C_f} \tag{4}$$

where

G : Charge amplifier gain [V/C]

Equation (5) expresses the relation between electrical charge, capacity and voltage in a capacitor.

$$V = \frac{Q}{C} \tag{5}$$

with

V : Voltage [V]
Q: Electrical charge [C]

C: Capacity [F]

The voltage at the amplifier's output is the voltage at the feedback capacitor, which is produced by the electrical charge moved by the sensor into the capacitor upon mechanical excitation.

This signal is finally connected to a National Instruments NI-6259 data acquisition board and custom-developed software based on Labview was used for signal acquisition, display and storage. The amplifier is supplied directly by the 5 V single-supply of the data acquisition board and is provided with a 2.5 V offset to allow symmetrical signals to vary around the offset.

After proper grounding and shielding, the sensors produced a low-noise signal, which was improved by implementing in the software a 10th-order bandstop filter with a stopband between 45 and 55 Hz to reduce 50 Hz-noise. With this setup the measurement system could represent even the smallest signals, in the order of a few mV, very accurately.

2.5.2 Experimental test setup

The filaments were subjected to tensile stress to test its functionality as a mechanical sensor. For deformations along the filaments, these were placed between the grips (distance between grips: 30 mm) in a *Shimadzu AG-IS 500 N* universal tensile testing machine (Figure 6), using a load cell of 1 kN. A pre-tension was applied with the objective of keeping the filament permanently under tension during the test. From the mechanical characterization performed, it was decided to apply 5 N of pre-tension, a value sufficient for the purpose and lying well in the linear region of the strain-stress curve. The tester was set to pull the filaments with a displacement of 0.3 mm, corresponding to 1% of extension. The pulling speed was set to 100 mm min^{-1} and 20 cycles were performed.

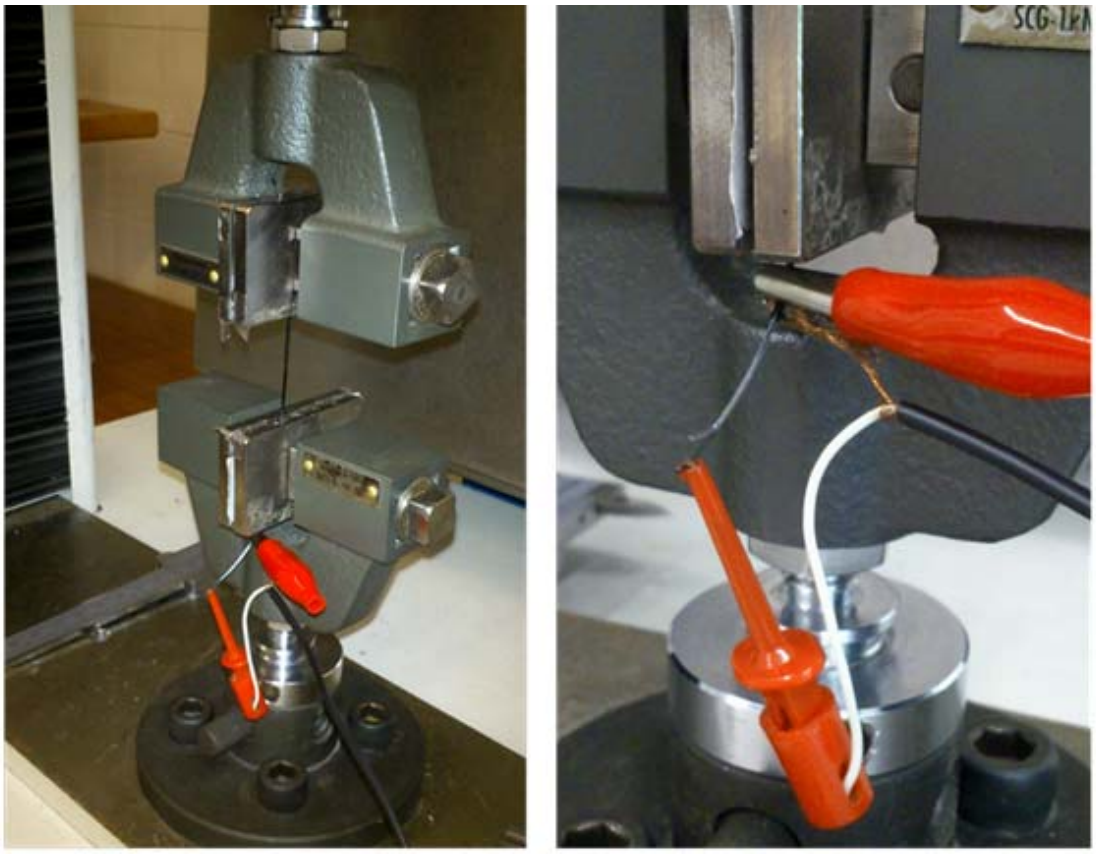

FIGURE 6 Test setup for stretching action (left), electrical connection detail (right)

3. RESULTS AND DISCUSSION

3.1. Extrusion

Figure 7 shows cross-section images of two samples of type 1 and type 2 filaments each. The filaments were inserted into resin, cut and polished.

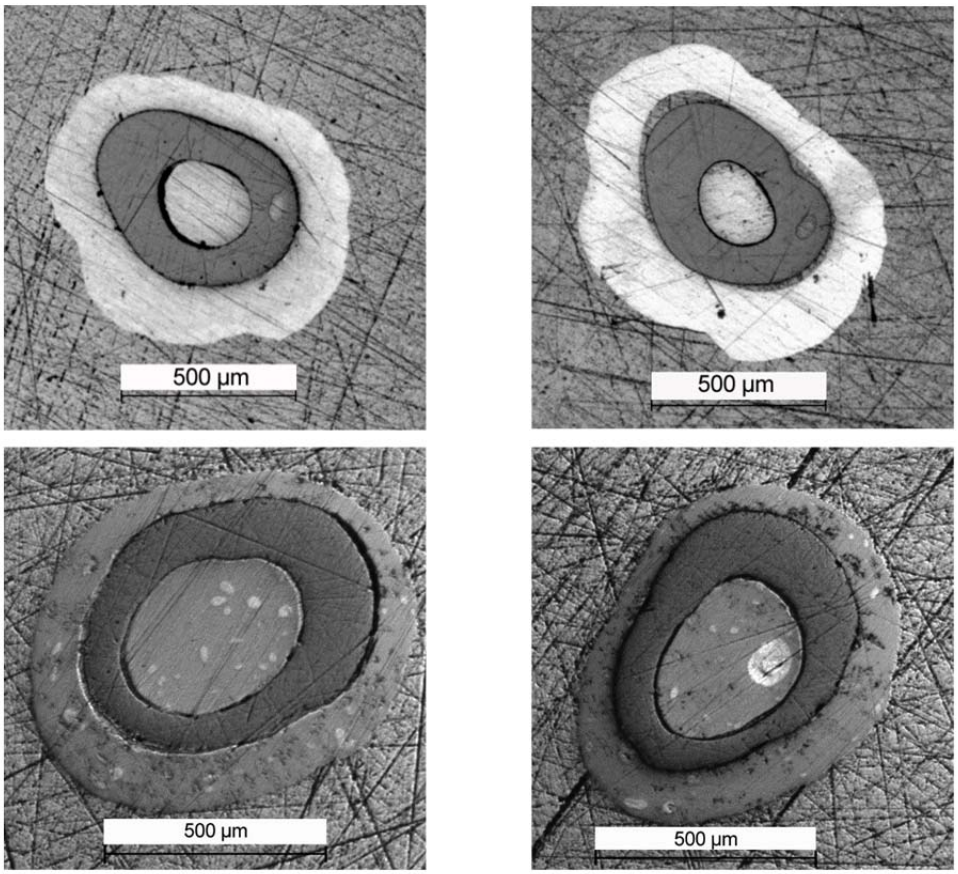

FIGURE 7 Microphotographs of the three-layer filament cross-section in two samples of filament type 1 (upper row) and two samples of filament type 2 (lower row).

As can be observed, the shape of the layers is not fully axisymmetric, with type 2 filaments exhibiting a more even geometry than type 1 filaments. Moreover, a larger trend for layer delamination is observed for type 1 filaments.

Although the modular design of the dye appeared as an interesting advantage of the extrusion die, fine interplay between the different modules is required, which revealed itself as a source of imprecision. The inexistence of a tuning mechanism and the complex rheological behavior of the materials employed, render process control very difficult to achieve, resulting in the obtained asymmetric layer distribution. Still, it was possible to obtain continuous layers of the different materials that comprise the filament, which assures electrical conductivity in the inner and outer layers, making it possible to pick up the electric signals generated in the piezoelectric layer.

A more even geometry of the filament would allow improvement in several aspects, among them the optimization of the poling procedure as, for example, the maximum electric field that can be applied, which is currently imposed by localized defects of the PVDF layer. However, an on-line tunable tool, required to handle different materials, layer thickness distribution and processing conditions, would have a prohibitive cost, not adequate for this phase of the investigation (proof of concept).

Another problem to be tackled is the lack of adhesion between the conductive and the electroactive areas, which can reduce the signal pick-up of the sensor and thus decrease its sensitivity and affect the homogeneity of behavior along the filament length. Although the void spaces visible in the microscopic images are most probably caused by the cutting and polishing actions used in sample preparation, they reveal a potential for layer delamination.

3.2 Poling fields

Table 2 summarizes the PVDF layer thickness measured from Figure 7, and under a voltage of 9 kV, the resulting poling field for the thickest and thinnest points of the PVDF layer.

TABLE 2 PVDF layer thickness and poling fields

Filament	Minimum thickness [μm]	Maximum thickness [μm]	Minimum field [MV m^{-1}]	Maximum field [MV m^{-1}]
Type 1	91	200	47	86
Type 2	47	160	56	190

3.3 ß-phase content

Figure 8 shows the FTIR spectrum obtained for the different filaments.

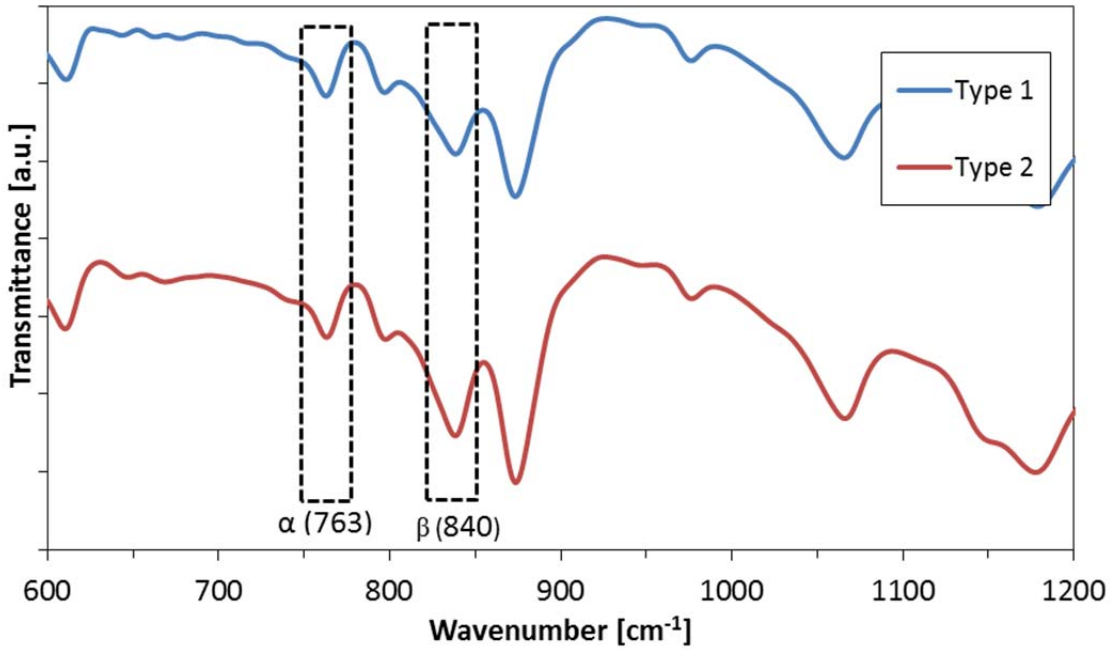

FIGURE 8 FTIR spectrum of the extruded samples

The calculation of ß-phase content according to Equation 2 yields the following result:

TABLE 3 ß-phase content of the samples

Filament	% ß-phase content	Standard deviation (%)
Type 1	59	3.6
Type 2	68	6.5

The value found for the type 1 filament is relatively low, considering that in previous experiments with PVDF extruded filament, piezoelectric phase contents of 70 to 80 % had been achieved.[20] Still, this percentage of ß-phase material is sufficient to obtain electroactive filaments, as will be presented in Section 3.4.

On the other hand, the value of approximately 68% found for the type 2 filament confirms that under the current dynamic processing conditions the high heater temperature is not inhibiting the achievement of electroactive phase material.

The higher values of ß -phase content obtained for the type 2 filaments are also related to the higher stretching ratio, which was 5, while the one achieved for the type 1 filaments was 4.

3.3 Mechanical test

Figure 9 shows the results of the tensile test.

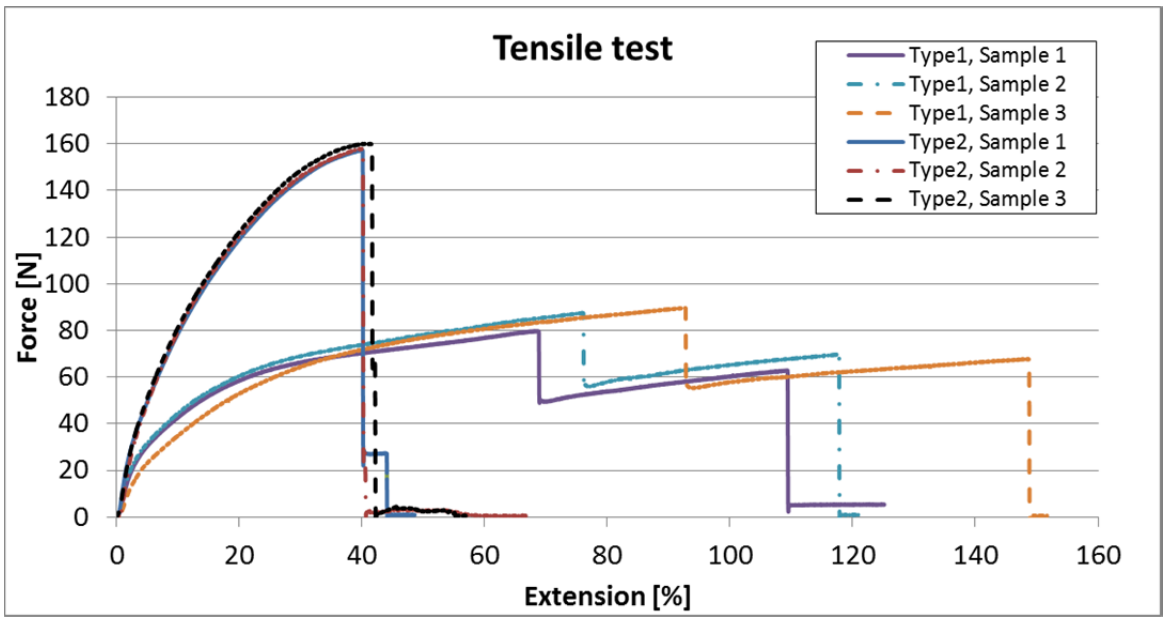

FIGURE 9 Tensile test on samples of the filaments

The graph in Figure 9 shows that type 2 filaments exhibit almost double the breaking strength of type 1 filaments. In both cases, rupture occurs at values that are much higher than the force ranges in which the filament sensor is expected to be used (lower than 20 N). Moreover, the filaments exhibit a linear stress-strain behaviour in this range. It can also be observed that the tensile modulus is higher for the filament type 2. The difference in mechanical behavior results mainly from the higher draw ratio used in filament type 2, as the cross-section area of both filaments is very similar.

Regarding type 1 filaments, layers break at different times. The outer layer is the first to break, followed by the PVDF intermediate layer, which then causes sample fracture.

For type 2 filaments a different behaviour is observed. These samples fully fracture almost immediately after the failure of the first layer, which is also the outer conductive layer. The mechanical properties of the layers seem in this case to be more balanced in terms of mechanical resistance.

Rupture of the innermost layer cannot be observed on the graph. This layer seems to be already broken when the PVDF layer breaks.

3.4. Electrical test

Figure 10 shows the force/displacement values measured by the universal tester and the electrical signals resulting from this excitation, for a sample of filament type 1.

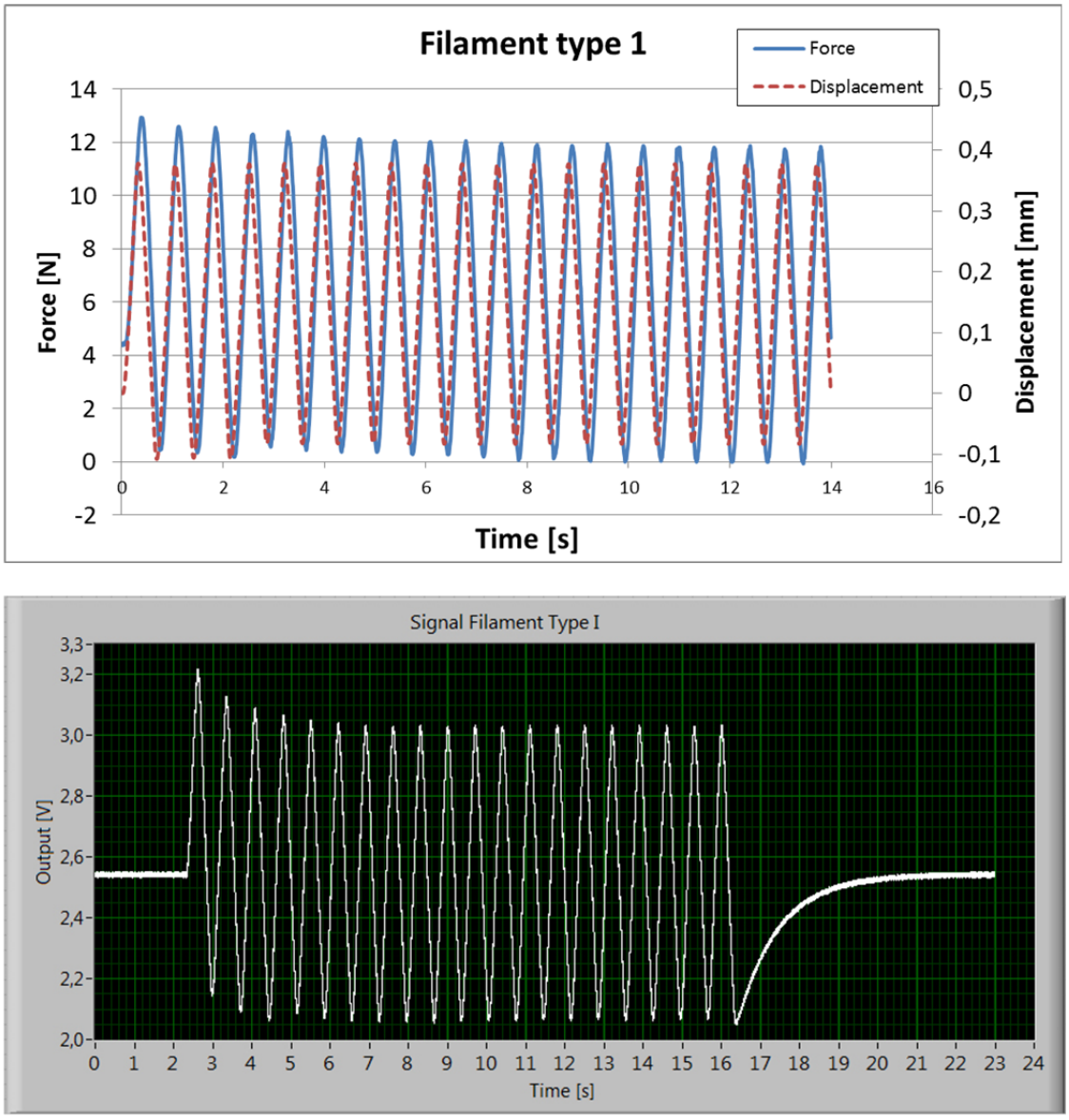

FIGURE 10 Force and displacement (upper graph) and electrical signal (lower graph) picked up by the measurement system during the cyclic test on one sample of filament type 1.

The same is shown in Figure 11 a sample of filament type 2.

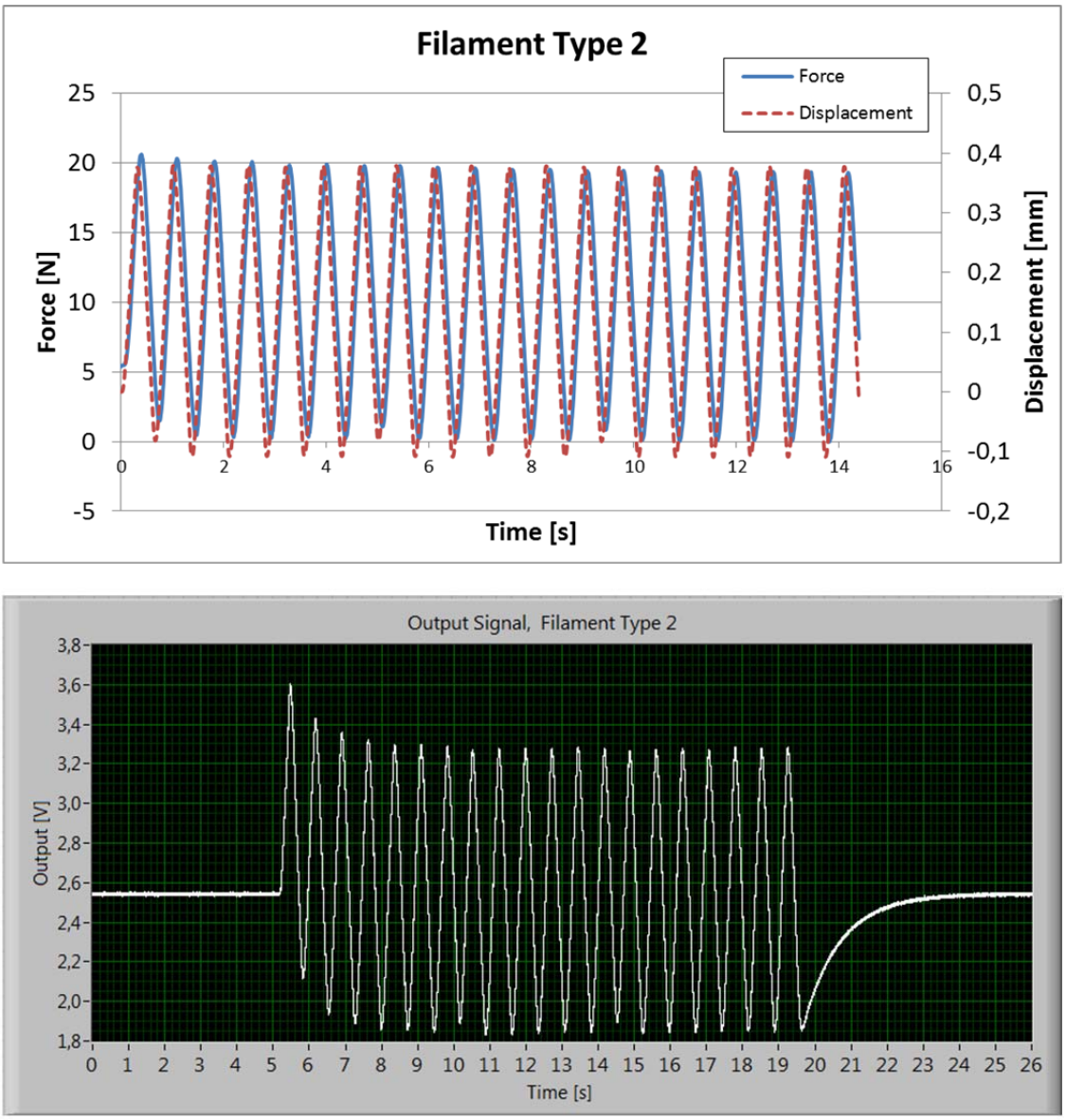

FIGURE 11 Force and displacement (upper graph) and electrical signal (lower graph) picked up by the measurement system during the cyclic test on one sample of filament type 2.

As shown in Figure 10 and Figure 11, the electrical response depicts the force variations very accurately, with the typical effects present on a piezoelectric sensor coupled to a charge amplifier, as explained in Section 2.5.1. The signal suffers a decay of average value caused by the high-pass response of the charge amplifier, which eliminates the

average values over time (the signal tends to the electrically produced 2.5 V offset). After the last cycle, the signal again converges to the 2.5 V offset. These two decays occur with a time constant that, in the current case and considering the values of C_f=10 nF and R_f=100 MΩ, is T=1 s, which is in accordance with the observed signals.

The peak-to-peak value of the electrical signal at cycle 11 for filament type 1 is 0.97 V, corresponding to a force variation of 11.78 N. Filament type 2 presents 1.44 V for 19.41 N. For these values, the sensitivities of the sensors are computed as follows:

The charge injected into the capacitor for a force range of 11.78 N in filament type 1 is

$$Q = V \cdot C = 0.97 \cdot 10 \cdot 10^{-9} = 9.7\ nC \tag{6}$$

For filament type 2 a value of 14.4 nC is obtained.

Thus, the sensitivity of the filament sensor type 1 can be calculated as

$$S = \frac{Q}{F} = \frac{9.7 \cdot 10^{-9} C}{11.78\ N} = 0.82 \frac{nC}{N} \tag{7}$$

The same calculation results in 0.75 nC N^{-1} for filament type 2.

For comparison purposes, a sensor based on commercial PVDF film (metallized film sheet from Measurement Specialties, 28 μm thickness), with approximately the same volume of PVDF, was prepared. A strip of the PVDF film with dimensions 30 mm x 7 mm was cut. The tensile testing machine was set to produce the same cyclic extension of 1 % in the longer direction of the strip and the electrical output of this sensor was measured using the same charge amplifier. The signal produced by this sensor was much higher and a feedback capacitor of 104 nF had to be used to lower the amplifier gain and avoid saturation. In this configuration, the measurement system produced 1.95 V for a force variation of 6.1 N. Repeating the calculation of Equations 6 and 7, the output of the film-based sensor results as 33.2 nC N^{-1}, which is an order of magnitude higher than that produced by the filaments.

Several factors should be taken into account to explain the difference in sensitivity of the filament sensors when compared to the film. In the first place, the ß-phase contents of 59 and 68% found in the filaments are lower. ß-phase content of 95% has been determined in poled piezoelectric film from the same manufacturer.[31] Second, poling fields achieved in this experiment are also low. Although they exceed the coercive field for optimal results a larger poling field is required.[1,11] To increase the poling field, a more even geometry of the filament has to be achieved. This would allow increasing the poling voltage. In combination with this, better results may be achieved by reducing the PVDF layer thickness.

A third issue that may affect the results obtained is the adhesion between the electrical conductive layers and the PVDF layer. As can be observed in Figure 7 there is a potential for layer delamination and the occurrence of voids between conductive layers and the electroactive layer. This affects the collection of the electrical charge moved to/from the surface of the PVDF by the piezoelectric effect, reducing the signal produced in the charge amplifier and thus decreasing sensitivity.

Considering the higher ß-phase content, poling field and slightly larger volume of electroactive material present in filament sensor type 2, a higher sensitivity from this sensor would be expected, which did not occur. Considering all the plausible factors for this fact, lack of layer adhesion is seen as a probable cause for sensitivity loss and should be improved in subsequent studies.

4. CONCLUSION

In this work, a proof-of-concept for a three-layered co-extruded filament sensor, produced in a continuous manner, has been given. The experimental characterisation performed showed that the sensor produces an electric signal proportional to the tensile force applied.

Conditions have been set for extrusion and drawing of the filaments in order to provide the electroactive layer with its piezoelectric properties. Two different types of materials for the conductive layers of the filaments have been tested. The electroactive phase (β-phase) content of the filaments has been measured using FTIR and found to be of 59 and 68 % for type 1 and type 2 filaments, respectively.

The filament has been tested under traction and its functionality as a sensor has been demonstrated. Three centimetres long filament segments exhibited a sensitivity of 0.82 and 0.75 nC N^{-1}. A sensor of approximately equal volume of PVDF based on a commercial PVDF film provided 33.2 nC N^{-1}. Albeit this difference, the filament sensor provides enough sensitivity to generate high quality signals suitable for the development applications.

Further work on optimization of the extrusion process can improve the sensitivity and geometry of the sensor. The reduction of the filament's cross-sectional dimensions can then lead to the mass-production of low-cost electroactive materials with possibility of full textile integration and interesting sensing capabilities and applications.

ACKNOWLEDGEMENTS

This work was supported by FEDER through the COMPETE Program and by the Portuguese Foundation for Science and Technology (FCT) by project PTDC/CTM/108801/2008 | FCOMP-01-0124-FEDER-009480 and in the framework of the Strategic Project PEst-C/FIS/UI607/20112011, PEst-C/CTM/LA0025/2013 (Strategic Project - LA 25 - 2013-2014) and PEst-C/CTM/UI0264/2011.

REFERENCES

1. Martins, P.; Lopes, A. C.; Lanceros-Mendez, S. *Prog. Polym. Sci.* **2013**, http://dx.doi.org/10.1016/j.progpolymsci.2013.07.006.
2. Bauer, S. *J. Appl. Phys.* **1996**, *80*, 5531-5559.

3. Nalwa, H. S. In Ferroelectric Polymers: Chemistry, Physics and Applications, Marcel Dekker, Inc: New York, **1995**.
4. Salimi, A.; Yousefi, A. A. *Polym. Test*. **2003**, *22*, 699-704.
5. Lanceros-Mendez, S.; Mano, J. F.; Costa, A. M.; Schmidt, V. H. *J. Macromol. Sci., Part B: Phys.* **2001**, *40*, 517-527.
6. Nakamura, K; Sawai, D.; Watanabe, Y; Taguchi, D.; Takahashi, Y.; Furukawa, T.; Kanamoto, T. *J. Polym. Sci. Part B: Polym. Phys.* **2003**, *41*, 1701-1712.
7. Lanceros-Mendez, S.; Moreira, M. V.; Mano, J. F.; Schmidt, V. H.; Bohannan, G. *Ferroelectrics.* **2002**, *273*, 15-20.
8. Matsushige, K.; Nagata, K.; Imada, S.; Takemura, T. *Polymer.* **1980**, *21*, 1391-1397.
9. Gregorio Jr., R.; Ueno, E. M. *J. Mater. Sci+* **1999**, *34*, 4489-4500.
10. Gregorio Jr., R.; Cestari, M. *J. Polym. Sci. Part B: Polym. Phys.* **1994**, *32*, 859-870.
11. Gomes, J.; Nunes, J. S.; Sencadas, V.; Lanceros-Mendez, S. *Smart. Mater. Struct.* **2010**, *19(6)*, 065010.
12. Sencadas, V.; Gregorio Jr., R.; Lanceros-Mendez, S. *J. Macromol. Sci., Part B: Phys.* **2009**, *48*, 514-525.
13. Dickens, B.; Balizer, E.; DeReggi, A. S.; Roth, S. C. *J. Appl. Phys.* **1992**, *72*, 4258-4265.
14. Dargaville, T.; Celina, M.; Elliott, J.; Chaplya, P.; Jones, G.; Mowery, D.; Assink, R.; Clough, R.; Martin, J. Characterization, Performance and Optimization of PVDF as a Piezoelectric Film for Advanced Space Mirror Concepts, SANDIA REPORT SAND2005-6846, Sandia National Laboratories, **2005**.
15. Piezo Film Sensors Technical Manual, Application Note, Measurement Specialties, Inc., **2008**, p.43. (available at http://www.meas-spec.com/product/t_resources.aspx?id=540#).
16. Moore Jr., E. P. In Polypropylene Handbook, 1st ed., Hanser: New York, **1996**.
17. Naficy, S.; Garmabi, H. *Compos. Sci. Technol.* **2007**, *67*, 3233-3241.
18. Hua, Z.; Ping, R.; Guifang, Z.; Changfa, X. *Journal of Wuhan University of Technology – Mater. Sci. Ed.* **2006**, *21(4)*, 53-55.
19. Steinmann, W.; Walter, S.; Seide, G.; Gries, T.; Roth, G.; Schubnell, M. *J. Appl. Polym. Sci.* **2011**, *120(1)*, 21-35.
20. Ferreira, A.; Costa, P.; Carvalho, H.; Nóbrega, J. M.; Sencadas, V.; Lanceros-Mendez, S. *J. Polym. Res.* **2011**, *18(6)*, 1653-1658.
21. Lund, A.; Hagström, B. *J. Appl. Polym. Sci.* **2011**, *120*, 1080-1089.
22. Janiczek, T. *J. Electrostatics*. **2001**, *51–52*, 167-172.
23. Mazurek, B.; Różecki, S.; Kowalzcyk, D. Proceedings of the 6th International Conference On Properlies and Applications of Dielelectric Materials, Xi'an Jiaotong University, China, 2000, 1041- 1044.
24. Mazurek, B.; Różecki, S.; Kowalczyk, D.; Janiczek, T. *J. Electrostatics*. ***2001,*** *51-52*, 180-185.
25. Vatansever, D.; Hadimani, R. L.; Shah, T.; Siores, E. In Piezoelectric Mono-Filament Extrusion for Green Energy Applications from Textiles, Proceedings of the International Congress of Innovative Textiles, ICONTEX2011, Istanbul, 2011.
26. Walter, S.; Steinmann, W.; Schütte, J.; Seide, G.; Gries, T.; Roth, G.; Wierach, P.; Sinapius, M. *Materials Technology: Advanced Performance Materials*. **2011**, *26 (3)*, 140–145.
27. Egusa, S.; Wang, Z.; Chocat, N.; Ruff, Z. M.; Stolyarov, A. M.; Shemuly, D.; Sorin, F.; Rakich, T.; Joannopoulos, J. D.; Fink, Y. *Nat Mater.* **2010**, *9*, 643-648.

28. Abouraddy, A. F.; Bayindir, M.; Benoit, G.; Hart, S. D.; Kuriki, K.; Orf, N.; Shapira, O.; Sorin, F.; Temelkuran, B.; Fink, Y. *Nat. Mater.* **2007**, *6*, 336-347.
29. Mano, J. F.; Costa, A. M.; Schmidt, V. H. **2001**, *40*, 517–527.
30. Gautschi, G. In Piezoelectric Sensorics: Force, Strain, Pressure, Acceleration and Acoustic Emission Sensors, Materials and Amplifiers, Springer-Verlag: Berlin, 2002.
31. Sencadas, V.; Costa, C. M.; Moreira, V.; Monteiro, J.; Mendiratta, S. K.; Mano, J. F.; Lanceros-Méndez, S. *e-Polymers.* **2005**, *2*.